NMR in Biomedicine

WILEY

NMR IN BIOMEDICINE

RESEARCH ARTICLE OPEN ACCESS

Neuromelanin Contrast Optimization and Improved Visualization of the Substantia Nigra in a 3D Gradient-Echo Sequence With Magnetization Transfer

Begoña Garate Andikoetxea[1,2] | Antonio Martín-Bastida[1,3] | Marta Vidorreta[4] | María Cruz Rodríguez-Oroz[1,3,5] | Lucas Soustelle[6] | Thomas Troalen[7] | Maria A. Fernández-Seara[8,5]

[1]Department of Neurology, Clínica Universidad de Navarra, Pamplona, Spain | [2]Universidad de Deusto, Bilbao, Spain | [3]Network Center for Biomedical Research in Neurodegenerative Diseases (CIBERNED), Madrid, Spain | [4]Siemens Healthineers, Madrid, Spain | [5]Instituto de Investigación Sanitaria de Navarra (IDISNA), Pamplona, Spain | [6]Aix Marseille Univ, CNRS, CRMBM, Marseille, France | [7]Siemens Healthcare SAS, Courbevoie, France | [8]Department of Radiology, Clínica Universidad de Navarra, Pamplona, Spain

Correspondence: Maria A. Fernández-Seara (mfseara@unav.es)

Received: 7 May 2025 | **Revised:** 29 July 2025 | **Accepted:** 31 July 2025

Funding: This work was supported by Siemens Healthineers.

Keywords: GRE | magnetization transfer | neuromelanin | substantia nigra | T1 | tissue properties

ABSTRACT

Neuromelanin (NM) magnetic resonance imaging has been used to evaluate the loss of melanized neurons in the substantia nigra, the main characteristic of Parkinson disease, typically by measuring the contrast ratio (CR) between the NM-rich areas and the cerebral peduncles in the midbrain. Neuromelanin contrast can be generated by employing a 3D gradient-echo (GRE) sequence with magnetization transfer (MT). In this work, we first evaluated the effect of the MT pulse frequency on the CR and contrast-to-noise ratio (CNR), analyzing a large frequency range from 500 to 100 KHz. Secondly, the impact of the 3D GRE sequence flip angle (FA) was evaluated using angles from 5° to 40°. Additionally, images were acquired both with and without MT for each FA, providing an opportunity to examine the effect of MT on tissue proton density, T1, and T2* values. Results showed that the highest CR and CNR were obtained for the lower MT frequencies (500–2000 Hz) and lower FAs (5°–10°). The lower FAs improved the visualization of the neuromelanin-rich area in the substantia nigra and facilitated delineating its volume. In addition, this work showed that the MT pulse decreased the T1 and PD of the tissue. Furthermore, simulations supported the obtained in vivo results.

1 | Introduction

Parkinson's disease not only stands as the second most prevalent neurodegenerative disorder globally, with a prevalence of more than 6 million patients, but its incidence has risen 2.5 times over the past 30 years [1]. Clinically, Parkinson's disease is characterized by the degeneration of dopaminergic neurons in the substantia nigra pars compacta (SN_{pc}), and the loss of dopaminergic innervation and dopamine in the striatum [2]. The predominant risk factor is advancing age, with men exhibiting 1.5-fold higher susceptibility. Additionally, extensive research has revealed a significant genetic predisposition, alongside the

Abbreviations: $B1_r$, B1 receiver field; $B1_t$, B1 transmit field; CNR, contrast to noise ratio; CR, contrast ratio; FA, flip angle; FSE/TSE, fast/turbo spin echo sequence; FWHM, full width at half-maximum; GM, grey matter; GRE, gradient echo; LC, locus coeruleus; MT, magnetization transfer; NM-MRI, neuromelanin-sensitive magnetic resonance imaging; PD, proton density; PD_{app}, PD apparent; PED, peduncles; ROI, region of interest; SAR, specific absorption rate; SN_{pc}, substantia nigra pars compacta; $T1_{app}$, T1 apparent; T1c, T1 corrected; TE, echo time; TI, inversion time; TR, repetition time; WM, white matter.

recognition of environmental and other contributing factors. Despite these advancements, the precise etiology of the disease remains elusive [1].

Diagnosis continues to be challenging due to the lack of definitive tests or biomarkers for early-stage detection. Consequently, clinical diagnostic precision remains suboptimal, and at the time symptoms appear, approximately 50% of melanized dopaminergic neurons in SN_{pc} have already died [3]. Some studies underlined that the dopaminergic loss was even higher, reaching 71% in the ventral tier area [4]. Neuromelanin-sensitive magnetic resonance imaging (NM-MRI) is considered an emerging biomarker of nigral depigmentation indexing the loss of melanized neurons, which has gained significant prominence as a potential non-invasive diagnostic technique in the last decade [5].

The pulse sequences used in NM-MRI have explored different sources of NM contrast: the T1 reduction attributable to paramagnetic NM-iron complexes, magnetization transfer (MT) effects based on different macromolecular content between the neuromelanin and the surrounding tissues, and spin density effects due to differences in water content [6]. The contrast enhancement may be attributed to either one of these sources or to several of them simultaneously.

The T1 reduction caused by neuromelanin is due to the interactions between the water nuclei of the tissue and the electron spins of the metallic components. Most of the sequences based on the T1 reduction effect have been used at 3T field strength instead of 1.5T as the signal to noise ratio is double, and T1 relaxation times are approximately between 1.2 and 1.3 times greater [7]. Several works have exploited this effect using T1-weighted 2D fast/turbo spin echo sequence (FSE/TSE) [8–10]. However, this type of multi-slice sequence also has MT effects due to the multiple refocusing pulses.

MT contrast is typically generated by applying an off-resonance pulse which causes the saturation of protons in macromolecules, which have short T2 values. These protons transfer magnetization to the bound and free water protons, some of which subsequently become saturated. When a second radio frequency pulse is applied, this time at the Larmor frequency of the free water protons, the signal obtained is reduced due to the previous saturation. This MT effect can be used to suppress the areas surrounding the neuromelanin, which are abundant in white matter (WM), as the macromolecular content in those areas is higher, and thus highlight the presence of the neuromelanin-rich areas that appear with greater signal intensity [11, 12].

Several studies have used this technique; however, there is little detailed information on the applied MT pulses, as most studies have used product sequences provided by the MRI manufacturers. Nakane et al. [13] used an off-resonance sinc pulse with a flip angle (FA) of 500° followed by a 3D gradient echo (GRE) sequence for imaging. Within their analyses, they evaluated the visibility of the neuromelanin-rich regions, underlining that visibility considerably increased when the MT pulse was applied. Ogisu et al. used an MT pulse at 600 Hz and a FA of 600° in addition to a TSE sequence to perform a NM volumetric analysis [14]. Van der Pluijm et al., in a three-sequence comparison, concluded that a 3D MT-GRE pulse sequence provided higher contrast compared with a 2D TSE sequence, as well as lower contrast variability [15]. Their MT pulse had an off-resonance frequency of 1200 Hz and a duration of 15.6 msec.

The MT pulse can be modulated by three main parameters: duration, amplitude, and frequency. Trujillo et al. [16] reported images obtained for different frequencies, from 1 to 100K Hz, where the variation of contrast with frequency was visible. Priovoulos et al. analyzed the impact of the MT pulse frequency on the NM contrast, evaluating frequencies from 210 Hz to 10K Hz, using a 3D multi-shot GRE sequence [17].

During the last decade, most of the groups that have employed MT sequences for NM-MRI have used GRE readouts with FAs of 20 [13] or 30 [18] degrees for the readout excitation pulses. Even though increasing the FA can enhance image contrast in T1-weighted sequences, recent works [12, 19] have noted that the maximum contrast between the NM and the peduncles (PED) in the SN was observed at lower FAs. This observation stemmed from the fact that the NM, akin to grey matter, is rich in water content; thus, it appeared bright against the suppressed signal of the peduncles. In other words, these works have introduced the idea of optimizing the NM contrast based on proton density (PD), using FAs smaller than the Ernst angle for a given repetition time (TR).

Some of the above-mentioned works analyzed NM contrast in both the SN and locus coeruleus (LC). The main reason for assessing the NM of the LC is that this structure is affected earlier during the disease progression compared to the SN and could potentially be used as an earlier biomarker of Parkinson disease [20]. In contrast, the main drawback of imaging the LC is its small size, which limits the reproducibility and reliability of the measurements. On the other hand, dopaminergic neuron loss in the SN is a hallmark of the disease, and several works have reported strong correlations between the NM loss and the severity of the motor symptoms that characterize Parkinson disease, as well as with the clinical scales used to identify the disease's characteristics [21]. Moreover, according to Liu et al., the optimal readout FA for the visualization of the LC may not be the same as the FA required to maximize the contrast in the SN [12]. Consequently, in this work, it was decided to prioritize the optimization of the SN contrast rather than the LC.

Observing the heterogeneity of the MT approaches previously used for neuromelanin imaging, the aim of this work was to perform a systematic study of the effects of two sequence parameters on the contrast ratio (CR) and contrast-to-noise ratio (CNR) between the neuromelanin and its surrounding structures, based on an MT sequence with off-resonance irradiation and 3D GRE readout. First, the effect of varying the MT pulse frequency was evaluated; subsequently, the effect of varying the FA of the GRE sequence was assessed. Additionally, images were acquired both with and without MT for each FA, providing an opportunity to examine tissue properties and quantify the reduction of T1 values of the different tissues associated with MT. Furthermore, simulations were conducted based on the experimental data to support the obtained in vivo results.

2 | Methods

2.1 | Sequence Optimization

As observed in the literature, most of the reported works did not vary the amplitude or the duration of the MT pulse, as these are constrained by Specific Absorption Rate (SAR) limits. Considering this, the first experiment of this work was based on varying the MT frequency, covering a wide range (500–100K Hz).

As an alternative and concurrent approach to sequence optimization, a second experiment employing various FAs (5°–40°) during the readout was conducted to quantify the effect of the FA on the neuromelanin contrast. Smaller FAs were expected to generate PD weighting, while larger FAs generated contrast based on T1 differences. The effect of the FA was evaluated for a frequency of 1200 Hz, selected based on the results of the first experiment. These data were used to measure tissue T1 (employed in the simulations) and to evaluate the T1 reduction effects of the MT pulse.

2.2 | Subject Recruitment and MRI Acquisition

The study was approved by the research ethics committee of the university and conducted in the university hospital. All participants gave informed consent prior to scanning. Exclusion criteria included: familial history of Parkinson's disease, neurological or psychiatric disorders, medical prescriptions for medications that could influence the outcomes, and MRI contraindications (e.g., cardiac pacemaker).

All healthy volunteers were scanned on a 3T MAGNETOM Skyra (Siemens Healthineers AG, Forchheim, Germany) using a 32-channel head coil.

The main sequences employed were an anatomical T1-weighted MPRAGE and the NM-sensitive 3D GRE with MT pulse. The MPRAGE anatomical images were used to position the 3D GRE slab perpendicular to the floor of the fourth ventricle and covering the midbrain and the basal ganglia. The parameters of the MPRAGE sequence, which lasted 5 min and 12 s, were: resolution = $1.0 \times 1.0 \times 1.1 mm^3$, 176 slices, acquisition matrix = $176 \times 248 \times 256$, TR = 2300 ms, echo time (TE) = 2.98 ms, inversion time (TI) = 900 ms, and FA = 9°.

The first experiment was performed in five healthy volunteers (26.80 ± 3.27 years, two females). The parameters of the 3D GRE sequence were: resolution = $0.9 \times 0.9 \times 1.0 mm^3$, 40 slices, acquisition matrix = $216 \times 288 \times 40$, TR = 53 ms, TE = 3.67 ms, and FA = 20°. The characteristics of the MT pulse were: sinc-shaped, duration = 10 ms, FA = 500°, and full width at half-maximum (FWHM) = 191.1 Hz. This sequence was run for six different MT frequencies: 500, 1500, 2000, 4000, 10K, and 100K Hz. The duration of the sequence was 5 min and 32 s.

Sixteen healthy controls (26.69 ± 3.75 years, 11 females) were recruited for the second experiment. The parameters of the 3D GRE sequence were the same as in the first experiment, except for the FA which was varied: 5°, 10°, 20°, 30°, and 40° and the acquisition of three echoes, with TE1 = 3.67 ms, TE2 = 10.51 ms, and TE3 = 17.35 ms (TR = 53 ms). For each FA, the sequence was run with and without the MT pulse. Thus, the 3D GRE sequence was performed 10 times for each subject. In addition, the main characteristics of the MT pulse were the same as for the first experiment with frequency = 1200 Hz.

2.3 | Image Processing

For each subject, NM-MRI images were co-registered using SPM 12 on Matlab R2023.a (MathWorks Inc., MA, USA). For region of interest (ROI) delineation only, images obtained for different frequencies in the first experiment and the MT ON and OFF scans for the second were averaged, so that the ROIs were delineated in the average images, not to be biased by a certain sequence.

2.3.1 | Contrast Ratio Measurements in the Substantia Nigra

The first echo images were used for the analysis of the CR and CNR between the neuromelanin pigmented region and the peduncles in the midbrain. The ROIs were delimited manually on the average images, in ITK-SNAP (Philadelphia, PA, USA). The same five slices were selected for each volunteer, starting with the third slice where the NM was observable, to cover the central slices where the neuromelanin containing regions were mainly visible. The NM ROI was defined based on patient morphology. Two square ROIs were drawn in each peduncle, of the same size (four voxels) in each slice, including a total of 16 voxels per slice. ROI locations and selected slices are illustrated in Figure 1A–D.

The CR was measured as

$$CR = \frac{\left(S_{NM} - S_{PED}\right)}{S_{PED}} \quad (1)$$

where S_{NM} and S_{PED} were the signal intensity of the NM pigmented region and the peduncle ROIs.

The contrast-to-noise ratio (CNR) was also evaluated. In these calculations, the signal intensity difference between the NM-rich region and the peduncles was divided by the standard deviation of the noise, which was measured in four circular ROIs located in the background outside the brain region, on the same slices used for the CR calculations.

2.3.2 | Volume Measurements

The volume of the NM pigmented region was measured in the images acquired in the second experiment. A total of 14 healthy controls were evaluated; two were excluded from the volume analysis due to movement and blood vessel artifacts. First, ROIs were manually drawn by two observers, starting from the first slice where the neuromelanin was visible, on a maximum of 10 slices, avoiding the outer slices where the signal of the NM

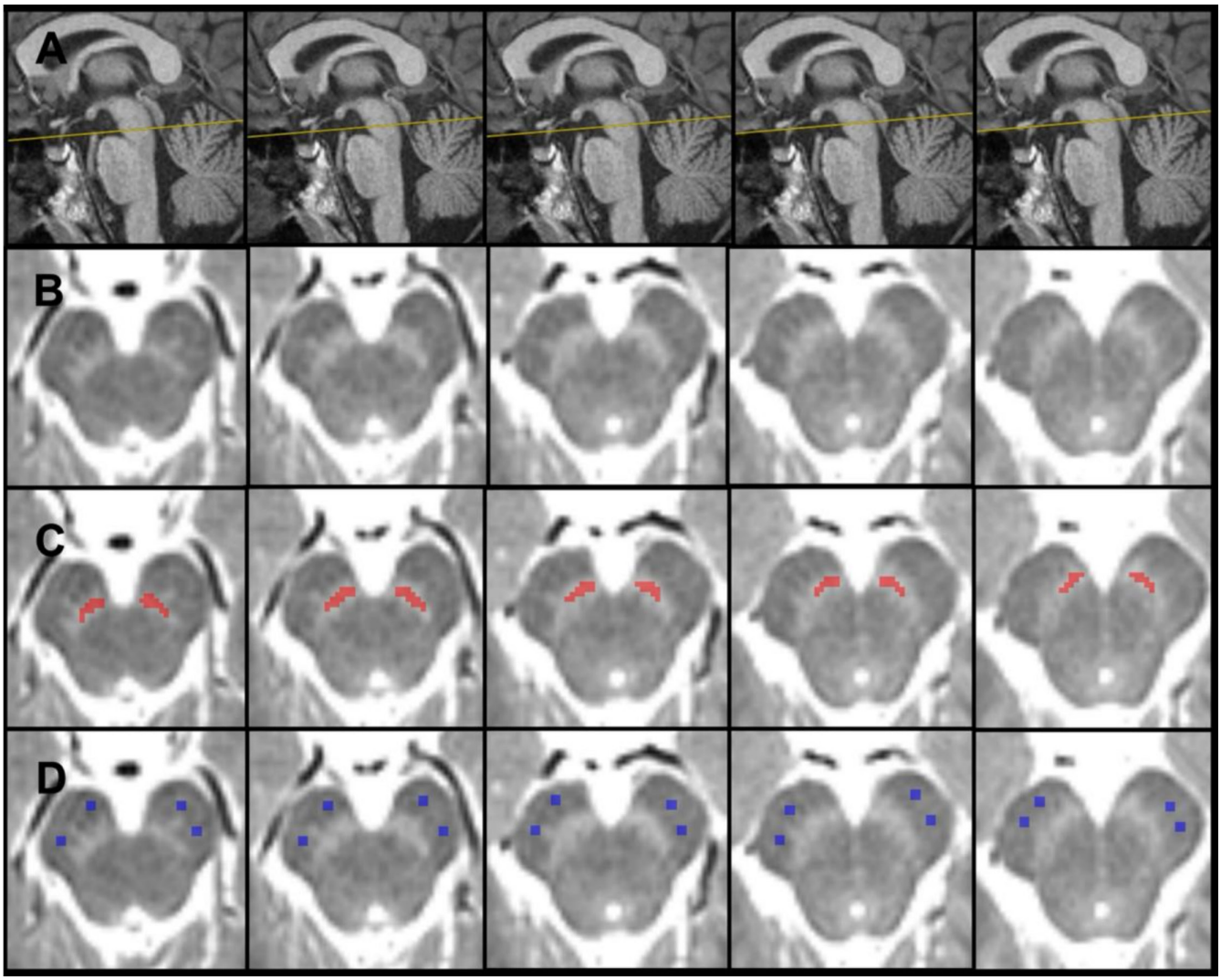

FIGURE 1 | Images acquired in a representative subject. (A) Location of the five slices (yellow lines) selected for contrast ratio measurements, shown over anatomical sagittal images. (B) The selected five slices for the contrast ratio measurements. (C) Delineated ROIs in the neuromelanin containing substantia nigra in red. (D) Delineated ROIs of the peduncles in blue for each slice.

pigmented area was affected by partial volume. The volumes measured by the two raters were averaged for each MT condition and FA.

2.3.3 | Tissue Properties Measurements and Signal Simulations

With the data from the second experiment, tissue properties (PD, T1, and T2*) were estimated to evaluate changes due to the MT effect. In addition, the estimated parameters were used to perform simulations of the tissue signal and CR for the different FAs to confirm the experimental results obtained in the FA comparison.

First T2* maps were calculated using the three echoes for each FA, with a two-parameter exponential fit, which yielded five T2* maps that were averaged to obtain a unique T2* map.

Subsequently, T1 and PD maps were computed using the first echo images for all the FAs ($\alpha = 5°$, 10°, 20°, 30°, and 40°) following a previously reported method [22], by fitting pixel-wise the imaging data to the signal equation:

$$S = PD_{app} \cdot sin(\alpha) \cdot \frac{1 - e^{-\frac{TR}{T1_{app}}}}{1 - cos(\alpha) \cdot e^{-\frac{TR}{T1_{app}}}} \cdot e^{-\frac{TE}{T2^*}} \quad (2)$$

Equation 2 represents the signal intensity for a short-TR spoiled GRE sequence, where α is the FA. T1 and PD values are denoted as apparent ($T1_{app}$ and PD_{app}) because their value is affected by B1 inhomogeneities, which determine the actual FA and introduce an error in the estimated parameters when they are calculated using the nominal FAs. The term $e^{-\frac{TE}{T2^*}}$ was computed based on the T2* obtained in the first step. These apparent values were corrected for the inhomogeneities of the B1 transmit field ($B1_t$), following the method described by Wang et al. [22], which allowed to calculate the B1t field from the acquired GRE data.

For low FAs and TR < T1, the following equations (Equations 3 and 4) give the PD effective (corrected for the inhomogeneities

of the B1t field, but not for the receiver ($B1_r$) field inhomogeneities) and T1 corrected values, deduced from the apparent values ($T1_{app}$ and PD_{app}) [22].

$$PD_{eff} = \frac{PD_{app}}{k} \quad (3)$$

$$T1_c = \frac{T1_{app}}{k^2} \quad (4)$$

Where k is the B1t field scale factor.

Equations 3 and 4 emphasize the necessity of B1 field inhomogeneity corrections, as a deviation of 10% in FA would result in a significant 19% error in the T1 value and 10% error in the PD. The final corrected PD value would be obtained after correcting for the $B1_r$ field inhomogeneities. In this work, this last *bias* correction was not considered essential. As the neuromelanin rich areas, (i.e., substantia nigra), and the peduncles are very close the coil sensitivity was not expected to vary considerably between these two regions.

Figure S1 illustrates the main outcomes of the correction method in a representative subject: $T1_{app}$ (Figure S1A), PD_{eff} (Figure S1D), $B1_t$ (Figure S1B), and $T1_c$ (Figure S1C) maps.

This procedure was applied to both MT ON and OFF datasets. Based on the maps obtained, the parameter values were measured on the previously detailed NM and PED ROIs. Two additional control ROIs were included: white matter (WM) and grey matter (GM) to ensure that the calculated tissue properties were within the range of values reported in the literature. These WM and GM ROIs were drawn in five consecutive slices where the basal ganglia were visible (Figure S2).

To confirm the experimental results obtained in the FA comparison, simulations were performed in MATLAB. Based on the group average tissue properties ($T1_c$, PD_{eff} and T2*), the signal was simulated as a function of FA, using equation 2, for the four tissue types (NM, PED, WM and GM), and the CR and CNR between NM and PED were calculated.

2.3.4 | Statistical Analysis

Data normality was assessed using Shapiro–Wilk tests. For normal data, parametric tests were employed, while non-normal data were analyzed using non-parametric tests. A p-value < 0.05 was considered significant.

To evaluate contrast differences due to the frequency of the MT pulse, CR measurements obtained in the first experiment were analyzed using a one-way analysis of variance (ANOVA) for repeated measures; followed by post hoc paired-t test, with Bonferroni correction. For the CNR, Friedman tests were used separately for MT ON and OFF data; followed by post hoc Wilcoxon signed-ranks test with Bonferroni correction.

To determine the impact of both the FA and the MT effect on the measured CR, a two-way ANOVA was used with two factors: MT condition with levels ON/OFF and FA with five levels. The ANOVA was followed by post hoc pairwise t-tests with Bonferroni correction. The same tests were applied to the volumetric data. For the CNR, Friedman test were used separately for MT ON and OFF data, followed by post hoc Wilcoxon signed-ranks test with Bonferroni correction.

In addition, to define the agreement between the segmentations performed by both observers, a Bland–Altman plot was generated, and DICE coefficients [23] were computed for each FA and MT condition.

Finally, to quantify the effect of MT on the tissue properties (T1, PD, and T2*), paired sample t-tests were used to compare each tissue property between MT conditions (ON vs. OFF). Bonferroni correction was applied to the p-values.

3 | Results

3.1 | Effect of the MT Pulse Frequency on the CR and CNR

Images of the central slice of the NM region obtained in a representative subject for all the different frequencies of the MT pulse are included in Figure 2A.

The obtained CR and CNR as a function of frequency is depicted in Figure 2B. All subjects showed the highest value for frequencies of 500, 1500, and 2000 Hz. The one-way repeated measures ANOVA showed significant differences across frequencies ($F = 46.70$, $p < 0.001$). The results of post hoc tests are included in Table S1. The lower frequencies of 500, 1500, and 2000 Hz did not show significant differences between them; however, they did show significant differences when they were compared with the higher frequencies of 4000, 10K, and 100K Hz. The results obtained for the CNR as a function of frequency are included in Table S4.

3.2 | Effect of the 3D GRE FA on the CR and CNR

Images obtained in a representative subject in experiment 2 (MT ON and OFF, with five different FAs) are depicted in Figure 3A,B.

Figure 4A shows the group averaged signal intensity in neuromelanin and peduncle ROIs and their CR, measured with and without MT, plotted as a function of GRE FA. Although the signal was largest for the 20° FA, the CR increased with decreasing FA and was highest for the FA = 5° (0.35 ± 0.04 (MT OFF) and 0.42 ± 0.06 (MT ON)). Although the MT pulse reduced the signal in both ROIs, it increased the CR for all FAs. The increase in contrast resulting from the MT effect remained consistent across FAs. It should be noted that the mean CR obtained with the MT pulse ON and a FA of 20° matched the average result obtained in the previous experiment, when the MT pulse frequency was low (MT frequencies of 500, 1500, and 2000 Hz). The results obtained for the CNR as a function of flip angle are included in the Figure 4B. The maximum CNR was obtained for the FA = 10° (81.69 ± 17.41 (MT OFF) and 79.28 ± 19.53 (MT ON)).

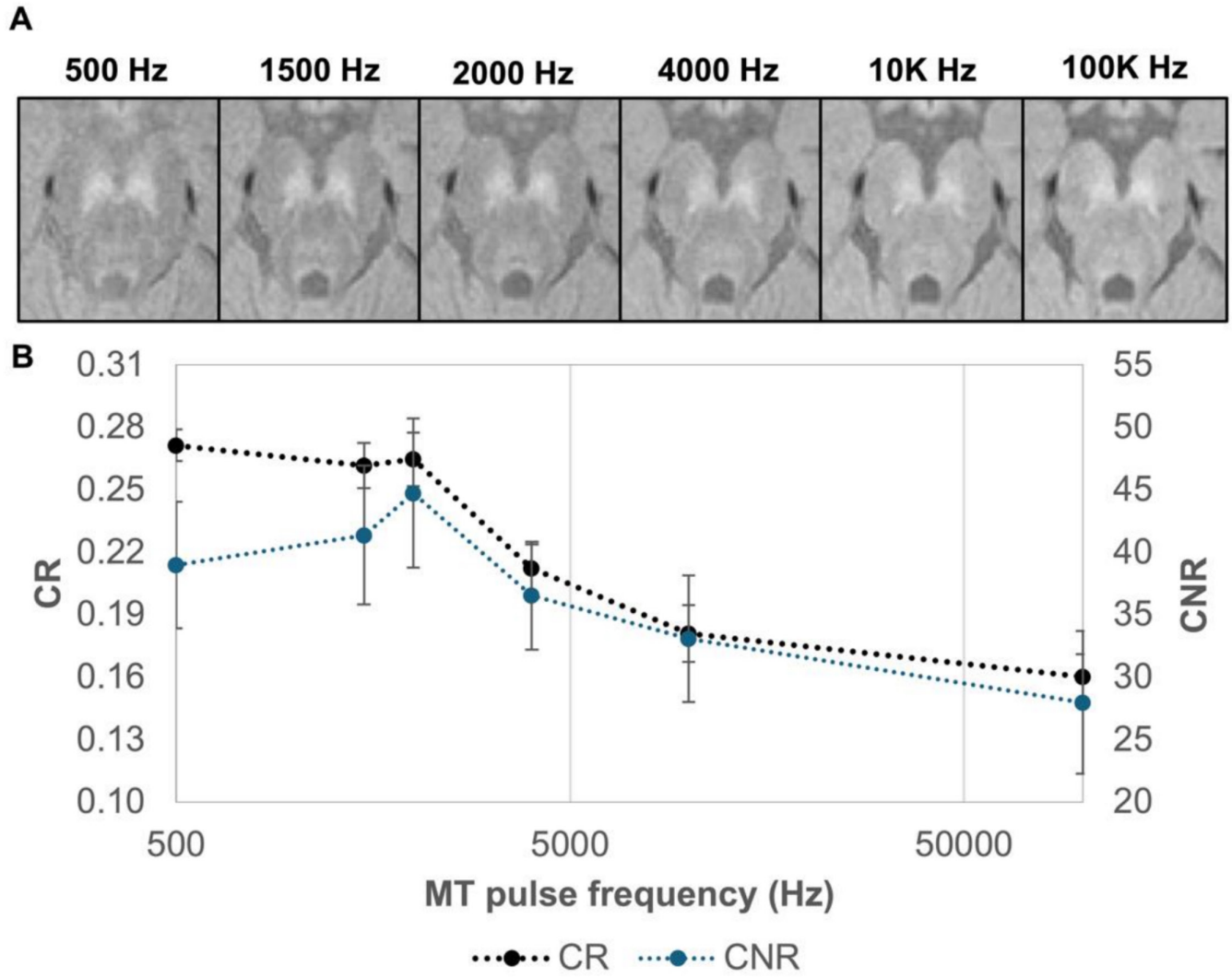

FIGURE 2 | Original images of the central slice of the NM pigmented region of a representative subject. (A) Obtained with the different frequencies (500, 1500, 2000, 4000, 10K, and 100K Hz) of the magnetization transfer pulse, in experiment 1. (B) Contrast ratios (CNR in blue and CR in black) obtained for all the analyzed MT frequencies expressed in logarithm scale in the five healthy controls. Error bars represent the standard deviation.

The results of the statistical analysis showed a significant main effect of FA ($F = 311.50$, $p < 0.001$), as well as a strong main effect of MT ($F = 207.07$, $p < 0.001$) in the CR, with no significant interaction ($F = 0.50$, $p = 0.733$). Post hoc tests showed significant differences for all the comparisons, except for the comparison between MT ON FA 5° and 10° ($p = 0.46$). The results for the post hoc tests are included in Tables S2 and S3. The CNR also showed a significant effect of FA ($p < 0.001$) and the post hoc tests showed significant differences for all the comparisons except for the comparison between MT ON FA 5° and 20° ($p = 0.49$), and between MT OFF FA 5° and 20° ($p = 0.50$) and 5° and 30° ($p = 0.62$). The results obtained for the post hoc tests for the CNR measurements are included in Tables S5 and S6.

3.3 | Volume Measurements

Figure 5A shows the NM pigmented region, on the five central slices imaged in a representative subject. Figure 5B shows the volumes of the NM pigmented regions segmented by the two raters for each FA, in MT ON and OFF conditions, their boxplots are displayed in the Figure 5C. The volumes were largest in the FA = 5° images acquired with MT ON across all subjects, averaging $599.01 \pm 42.26\,mm^3$ between both raters. For this FA, the CR was the highest, which improved the visualization of the NM content of the SN. The volume measured without MT for the same FA = 5° was $552.80 \pm 39.43\,mm^3$. Volumes measured by each rater are included in Table 2.

The statistical analysis showed a significant effect of FA ($F = 792.58$, $p < 0.001$) and MT ($F = 143.04$, $p < 0.001$), with no interaction ($F = 1.98$, $p = 0.101$). Moreover, the pairwise *t*-tests with Bonferroni correction were all significant (Tables S7 and S8).

The DICE coefficients included in Table 1 showed high agreement between raters for lower FAs. A Bland–Altman plot has also been included in Figure S4 to illustrate visually the inter-rater agreement.

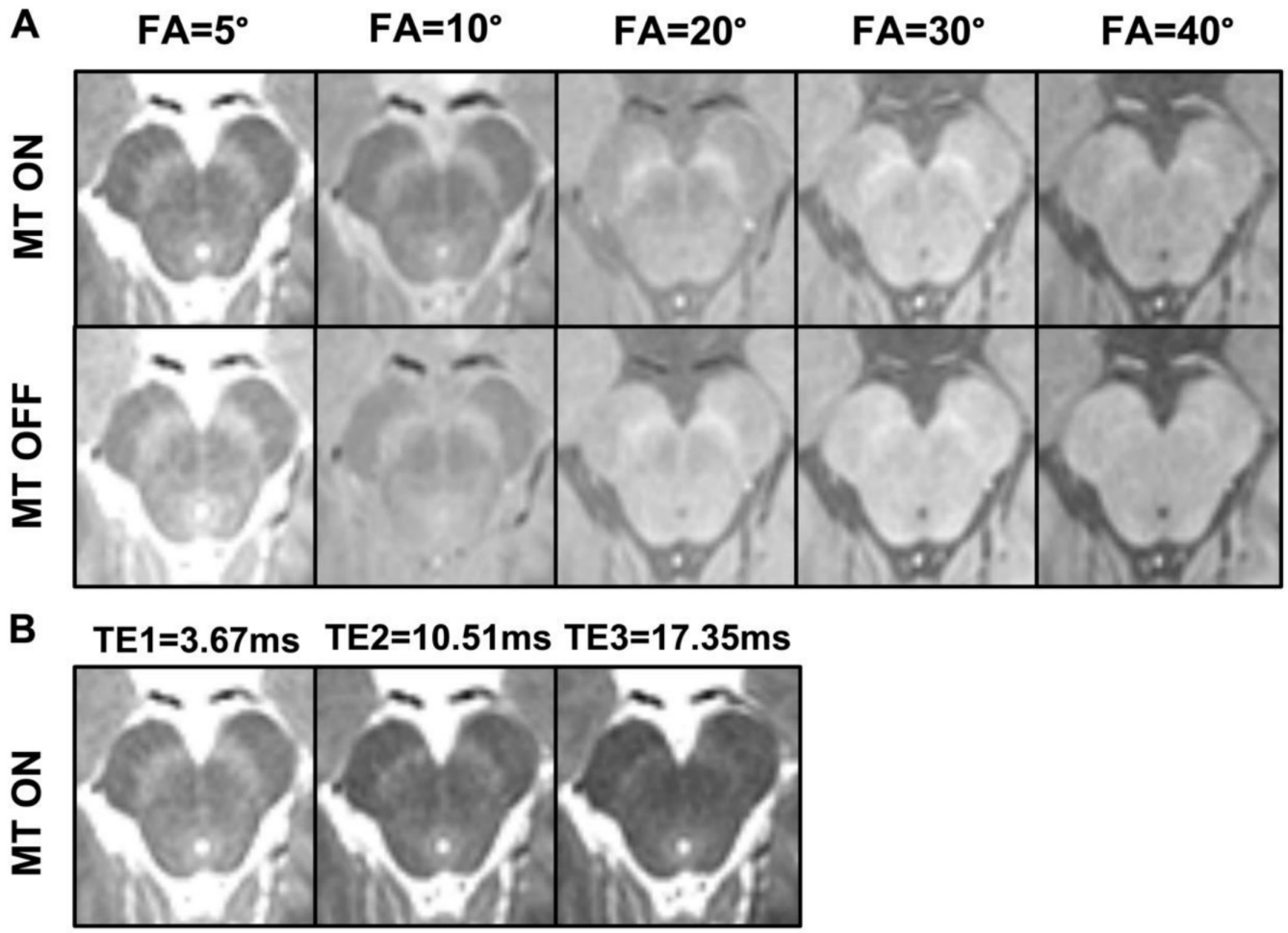

FIGURE 3 | Original images of the middle slice of the NM pigmented region of a representative subject, obtained in experiment 2. (A) MT ON (first row) and OFF (second row) first echo images obtained for each flip angle (5, 10, 20, 30, and 40). (B) First, second and third echo images (TEs = 3.67, 10.51, and 17.35 ms), obtained with the flip angle of 5°, and MT ON.

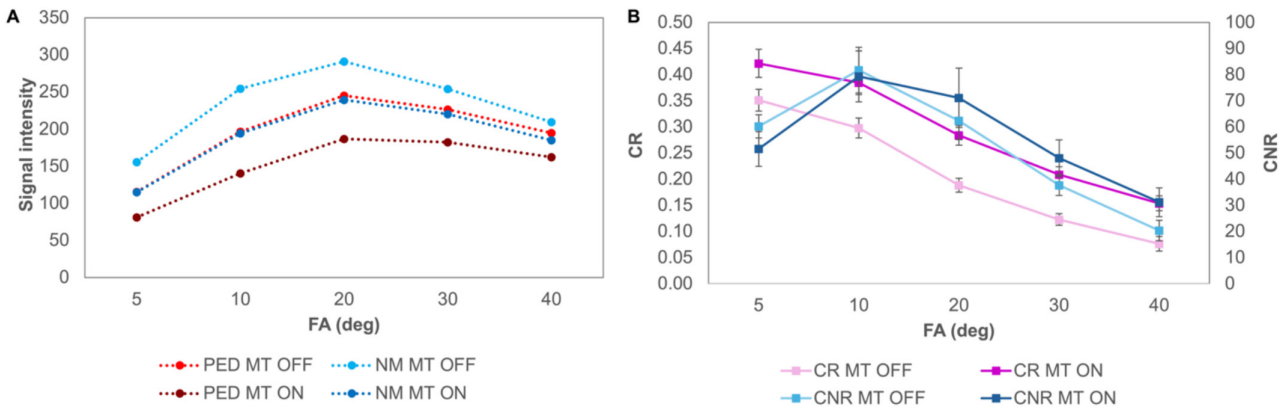

FIGURE 4 | Experimental signal intensities in the neuromelanin and peduncle regions (A), their contrast ratio and contrast to noise ratio (B) measured with and without magnetization transfer, plotted as a function of GRE flip angle. The error bars represent the standard deviation.

3.4 | Tissue Properties

The tissue properties (T1, PD and T2*) for the PED, NM, WM, and GM are detailed in Table 2.

The values for T1 and PD exhibited a significant decrease with MT for all tissues (all $p < 0.001$); Figure 6. In the case of T1 values, the reduction amounted to approximately 20%, while for PD values, it was close to 30%. The T2* MT ON and OFF values were not significantly different (PED $p = 0.72$, NM $p = 0.85$, WM $p = 1$ and GM $p = 0.86$).

The simulated signal intensities are illustrated in Figure 7. These simulation results aligned with the experimental

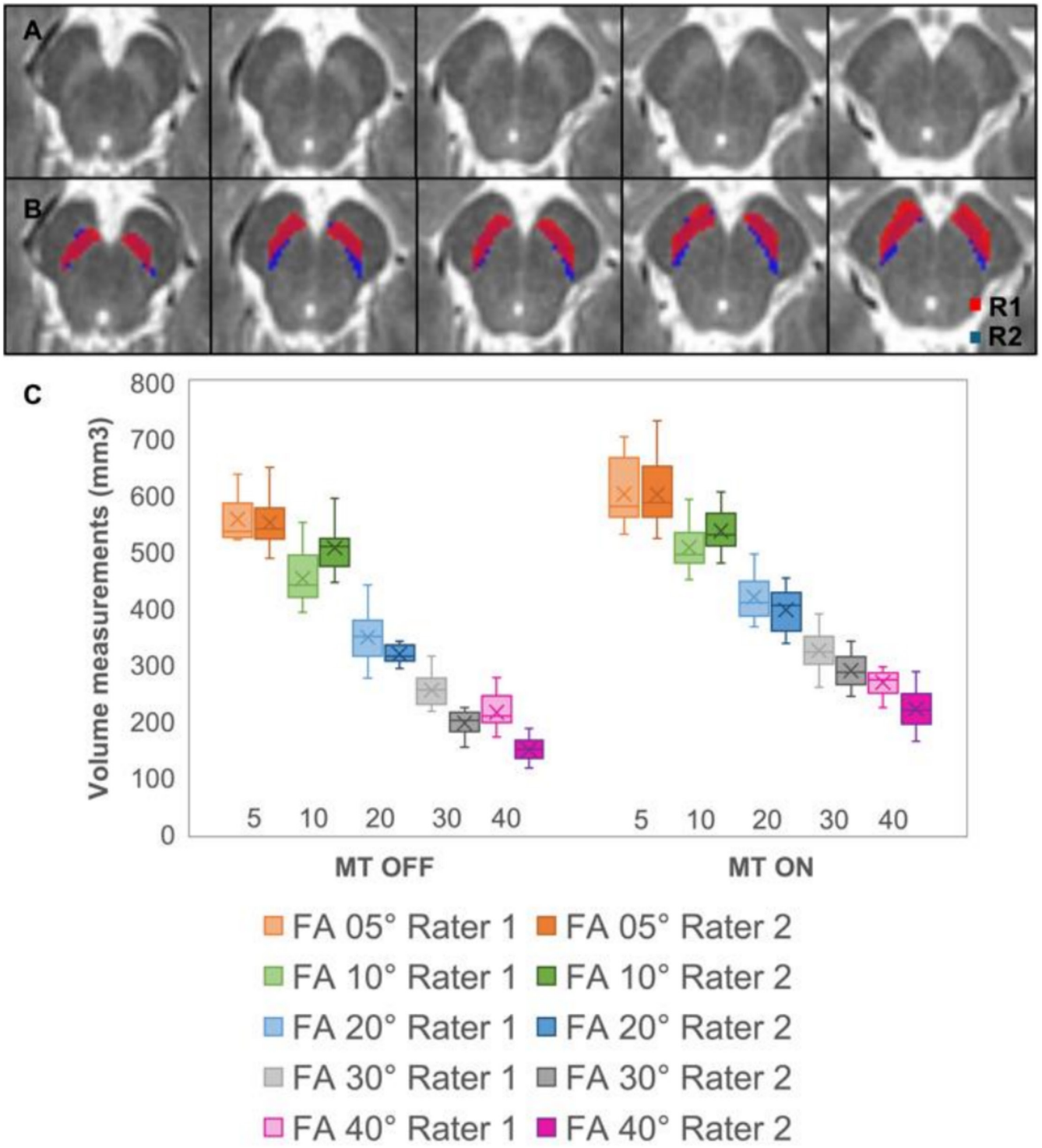

FIGURE 5 | NM pigmented regions of both raters. (A) Five consecutive central slices of a representative subject. (B) Segmentations of the regions defined by each rater (R1 and R2) on the five consecutive slices displayed on the top row. (C) Box plots of the Neuromelanin-rich area volume measurements for each flip angle (5, 10, 20, 30, and 40 deg), MT condition (ON, OFF) and rater (R1 and R2).

measurements, both in signal intensities, CR (Figure 7A,C) and CNR (Figure 7D).

4 | Discussion

The experiments conducted in this study demonstrated that off-resonance irradiation at lower offset frequencies resulted in higher MT contrast, with no significant differences observed between 500, 1500, and 2500 Hz. Additionally, the lower GRE FAs (5° and 10°) yielded the highest contrast. Moreover, the 5° FA in the MT ON condition also corresponded to the largest measured NM-rich region volume and the highest inter-rater agreement in the volume assessment. Furthermore, our findings showed that tissue properties (T1 and PD) decreased in the presence of MT. These experimental findings were supported by simulations.

TABLE 1 | Mean ± standard deviation of the volumes measured by each rater (R1 and R2) and DICE coefficient between raters for each flip angle and MT on and off.

	Volume measurements					
	MT ON			MT OFF		
Flip angle (deg)	R1	R2	DICE coefficient	R1	R2	DICE coefficient
5	595.91 ± 47.71	602.11 ± 58.86	0.75 ± 0.04	553.71 ± 37.75	551.89 ± 46.79	0.76 ± 0.04
10	502.44 ± 34.45	536.83 ± 36.41	0.72 ± 0.18	446.88 ± 37.41	507.29 ± 37.52	0.74 ± 0.03
20	416.04 ± 35.71	397.00 ± 38.10	0.71 ± 0.03	341.99 ± 40.50	318.79 ± 15.78	0.64 ± 0.05
30	330.71 ± 36.82	289.72 ± 27.89	0.65 ± 0.04	254.04 ± 28.78	196.79 ± 21.61	0.56 ± 0.06
40	276.59 ± 32.92	221.64 ± 33.56	0.62 ± 0.05	217.51 ± 28.16	149.34 ± 20.94	0.47 ± 0.07

TABLE 2 | Corrected tissue properties for the peduncle, neuromelanin, white matter and grey matter regions, after applying the STAGE correction method. Values expressed as mean ± SD for the evaluated five slices.

	T1c (ms)		PDeff		T2*app (ms)	
Tissues	MT OFF	MT ON	MT OFF	MT ON	MT OFF	MT ON
PED	955.55 ± 70.76	753.71 ± 63.96	1596.62 ± 133.50	1086.56 ± 118.55	50.72 ± 5.59	53.51 ± 5.05
NM	1258.53 ± 109.52	938.81 ± 82.67	2166.63 ± 316.55	1608.78 ± 175.73	39.10 ± 3.97	39.85 ± 4.21
WM	1017.58 ± 72.91	790.98 ± 62.77	1669.04 ± 137.24	1143.95 ± 133.35	45.43 ± 2.97	46.41 ± 2.83
GM	1608.77 ± 96.39	1218.21 ± 99.66	2236.39 ± 170.27	1545.06 ± 173.25	52.01 ± 5.28	54.06 ± 6.05

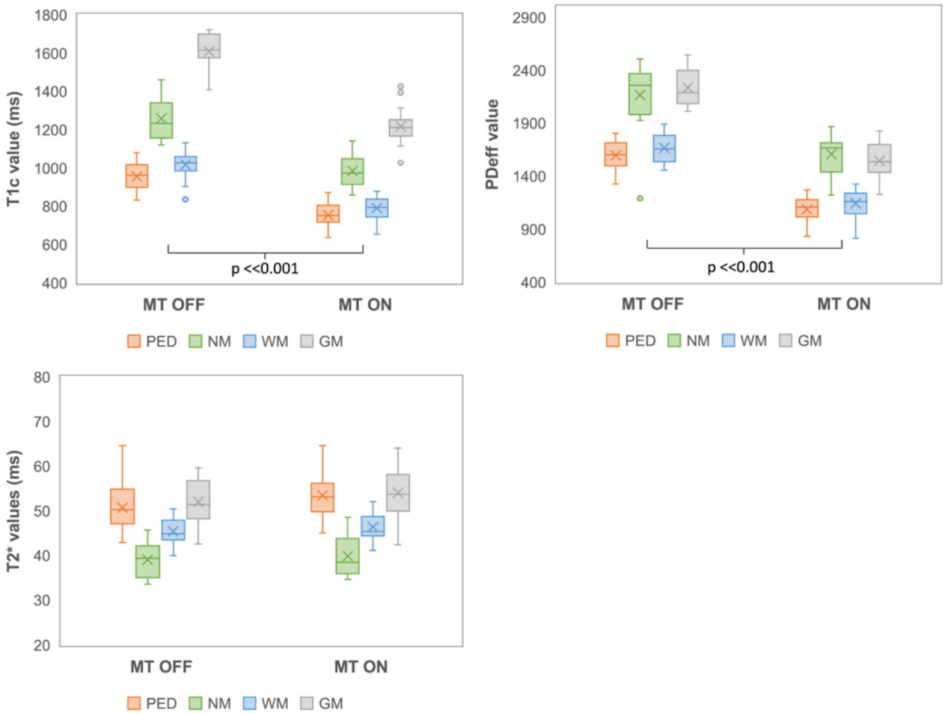

FIGURE 6 | Boxplots of the tissue properties ($T1_c$, PD_c and T2*) for each tissue with and without magnetization transfer, considering the 16 healthy controls.

The first experiment helped to understand the effect of the off-resonance MT pulse frequency, concluding that lower frequencies resulted in higher CR and CNR between the NM-rich areas and peduncles. Accordingly, Trujillo et al. [24] showed the same tendency in their data reporting the maximum CR for the MT frequencies around 1000 Hz, also using a 3D spoiled GRE sequence. In addition, Priovoulos et al. [17] underlined that the maximum contrast was qualitatively observed for

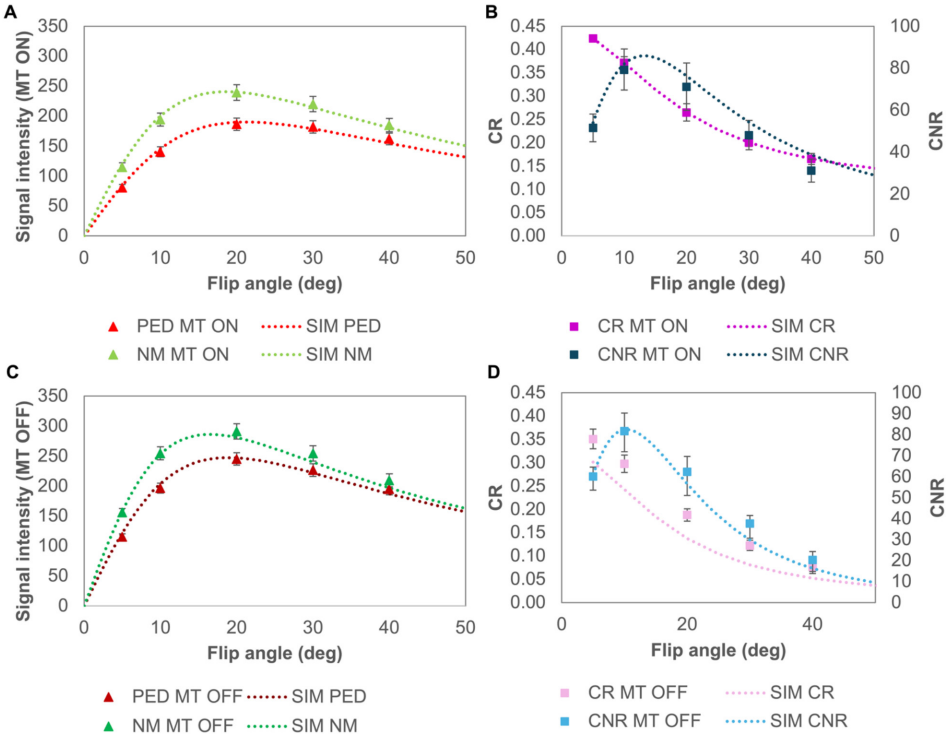

FIGURE 7 | Signal intensity in the NM and PED ROIs, as a function of flip angle for both experimental and simulated data (A and C), the corresponding contrast ratio (CR) and contrast to noise ratio (CNR) with (B) and without (D) MT. Simulated data are illustrated as dotted lines, while the triangles and squares represent the experimental data. The error bars represent the standard deviation.

frequencies between 860 and 4280 Hz. Moreover, in our experiment, we showed that for low frequencies (500, 1500, and 2000 Hz) there were no significant differences in contrast. Based on these results, we used the frequency of 1200 Hz for the second experiment.

The second experiment was designed to evaluate the effect of the GRE readout FA. Several works have used the CNR to evaluate the NM contrast enhancement [16, 12, 19]. Liu et al. [12] emphasized the benefits of low FAs for the visualization of the neuromelanin in the SN_{pc} after analyzing several angles. Our CNR calculations showed the highest experimental CNR for the 10° FA (both for MT on and off), while no significant differences were found between the 5° and 20° FAs. The maximum CR was also obtained for the lower FAs (5°–10°). This CR is also commonly employed in neuromelanin-sensitive MRI studies to enhance robustness and comparability [9, 10], and it has also been used to optimize the acquisition [13, 15, 24]. These results showed that the highest CNR and CR measurements were obtained with low flip angles, in agreement with previous studies.

Besides this, when volumes were measured by two raters, the highest levels of agreement were obtained for the cases of MT ON and lowest angle, which demonstrates likewise that the highest qualitative contrast was observed for the FA = 5°, helping with the delineation of the NM-rich areas and resulting in the highest volumes. This result is in agreement with recent work by Peng Liu et al. showing that even lower flip angles could be used to visualize the NM-rich area of the SN, without MT pulses.

The T1 values obtained for MT OFF in grey and white matter match with reported values [7, 25]. The T1 values in PED are slightly lower than white matter, while the T1 values in SN are lower than GM. In this work, it was observed that the measured T1 and PD values of all the tissues analyzed decreased with the application of the MT pulse. The decrease in PD values was expected. However, little has been reported on the effect of MT on T1 values. The measured values with MT were reduced by approximately 20% with respect to the MT OFF condition. Liu et al. [12] cited values of 670 and 910 ms as the T1 constraints of the WM and GM when the MT was ON, values that are lower than those reported in this work; however, they used an on-resonance MT binomial pulse scheme, which could explain the difference. Hua et al. measured decreased T1 values in mixed turbo spin echo sequences with increasing number of slices, showing that magnetization transfer effects, caused by excitation of adjacent slices, led to decreased T1 values [26]. Moreover, Hilbert et al. studied the effects of MT in MR fingerprinting, observing that calculated T1 values were reduced if the MT effect was not included in the model and increased by accounting for MT [27].

We acknowledge the limitations of this study. First, only young healthy subjects were included in both experiments. Further studies with subjects of different ages would help us understand the tendency of the NM-rich area volume and contrast according to age [28]. Secondly, the sequence was only optimized based on the results obtained on the SN_{pc}; this could be extended to the LC as several works have obtained different conclusions according to the analyzed brain structure.

5 | Conclusions

In conclusion, this work showed that the largest contrast ratio was observed for the 500 and 1500 Hz frequencies. In addition, the highest CR was obtained for the readout FA = 5° and MT ON, which also facilitated volume delineation of the NM-rich areas, showing the highest agreement between the two raters. Moreover, the highest CNR was obtained for the readout FA = 10° and MT ON, concluding that the lower FAs enhanced the NM contrast. Finally, this study showed how the MT pulse decreased both the T1 and PD tissue values.

Author Contributions

All authors contributed to the conception and design of the study. Begoña Garate Andikoetxea performed the data acquisition, analysis, and drafting of the manuscript. All authors contributed to the interpretation of the data and provided critical revisions. Maria A. Fernández-Seara supervised the project. All authors reviewed and approved the final version of the manuscript.

Acknowledgements

The greMT sequence used in the MT frequency analysis was provided by the CRMBM laboratory (Aix Marseille University, CNRS) and is available on Siemens' C2P platform.

Data Availability Statement

The data that support the findings of this study are available from the corresponding author upon reasonable request.

References

1. E. Tolosa, A. Garrido, S. W. Scholz, and W. Poewe, "Challenges in the Diagnosis of Parkinson's Disease," *Lancet Neurology* 20, no. 5 (2021): 385–397, https://doi.org/10.1016/S1474-4422(21)00030-2.

2. M. T. Hayes, "Parkinson's Disease and Parkinsonism," *American Journal of Medicine* 132, no. 7 (2019): 802–807, https://doi.org/10.1016/j.amjmed.2019.03.001.

3. E. C. Hirsch, S. Hunot, P. Damier, and B. Faucheux, "Glial Cells and Inflammation in Parkinson's Disease: A Role in Neurodegeneration?," *Annals of Neurology* 44, no. S1 (1998): S115–S120, https://doi.org/10.1002/ana.410440717.

4. J. M. Fearnley and A. J. Lees, "Ageing and Parkinson's Disease: Substantia Nigra Regional Selectivity," *Brain* 114, no. 5 (1991): 2283–2301, https://doi.org/10.1093/brain/114.5.2283.

5. N. He, Y. Chen, P. A. LeWitt, F. Yan, and E. M. Haacke, "Application of Neuromelanin MR Imaging in Parkinson Disease," *Journal of Magnetic Resonance Imaging* 57, no. 2 (2023): 337–352, https://doi.org/10.1002/jmri.28414.

6. T. Watanabe, X. Wang, Z. Tan, and J. Frahm, "Magnetic Resonance Imaging of Brain Cell Water," *Scientific Reports* 9, no. 1 (2019): 5084, https://doi.org/10.1038/s41598-019-41587-2.

7. J. P. Wansapura, S. K. Holland, R. S. Dunn, and W. S. Ball, "NMR Relaxation Times in the Human Brain at 3.0 Tesla," *Journal of Magnetic Resonance Imaging* 9, no. 4 (1999): 531–538, https://doi.org/10.1002/(SICI)1522-2586(199904)9:4<531::AID-JMRI4>3.0.CO;2-L.

8. D. García-Lorenzo, C. Longo-Dos Santos, C. Ewenczyk, et al., "The Coeruleus/Subcoeruleus Complex in Rapid Eye Movement Sleep Behaviour Disorders in Parkinson's Disease," *Brain* 136, no. 7 (2013): 2120–2129, https://doi.org/10.1093/brain/awt152.

9. M. Sasaki, E. Shibata, K. Tohyama, et al., "Neuromelanin Magnetic Resonance Imaging of Locus Ceruleus and Substantia Nigra in Parkinson's Disease," *Neuroreport* 17, no. 11 (2006): 1215–1218, https://doi.org/10.1097/01.wnr.0000227984.84927.a7.

10. E. Shibata, M. Sasaki, K. Tohyama, et al., "Use of Neuromelanin-Sensitive MRI to Distinguish Schizophrenic and Depressive Patients and Healthy Individuals Based on Signal Alterations in the Substantia Nigra and Locus Ceruleus," *Biological Psychiatry* 64, no. 5 (2008): 401–406, https://doi.org/10.1016/j.biopsych.2008.03.021.

11. R. M. Henkelman, G. J. Stanisz, and S. J. Graham, "Magnetization Transfer in MRI: A Review," *NMR in Biomedicine* 14, no. 2 (2001): 57–64, https://doi.org/10.1002/nbm.683.

12. Y. Liu, J. Li, N. He, et al., "Optimizing Neuromelanin Contrast in the Substantia Nigra and Locus Coeruleus Using a Magnetization Transfer Contrast Prepared 3D Gradient Recalled Echo Sequence," *NeuroImage* 218 (2020): 116935, https://doi.org/10.1016/j.neuroimage.2020.116935.

13. T. Nakane, T. Nihashi, H. Kawai, and S. Naganawa, "Visualization of Neuromelanin in the Substantia Nigra and Locus Ceruleus at 1.5T Using a 3D-Gradient Echo Sequence With Magnetization Transfer Contrast," *Magnetic Resonance in Medical Sciences* 7, no. 4 (2008): 205–210, https://doi.org/10.2463/mrms.7.205.

14. K. Ogisu, K. Kudo, M. Sasaki, et al., "3D Neuromelanin-Sensitive Magnetic Resonance Imaging With Semi-Automated Volume Measurement of the Substantia Nigra Pars Compacta for Diagnosis of Parkinson's Disease," *Neuroradiology* 55, no. 6 (2013): 719–724, https://doi.org/10.1007/s00234-013-1171-8.

15. M. van der Pluijm, C. Cassidy, M. Zandstra, et al., "Reliability and Reproducibility of Neuromelanin-Sensitive Imaging of the Substantia Nigra: A Comparison of Three Different Sequences," *Journal of Magnetic Resonance Imaging* 53, no. 3 (2021): 712–721, https://doi.org/10.1002/jmri.27384.

16. P. Trujillo, P. E. Summers, A. K. Smith, et al., "Pool Size Ratio of the Substantia Nigra in Parkinson's Disease Derived From Two Different Quantitative Magnetization Transfer Approaches," *Neuroradiology* 59, no. 12 (2017): 1251–1263, https://doi.org/10.1007/s00234-017-1911-2.

17. N. Priovoulos, S. C. J. van Boxel, H. I. L. Jacobs, et al., "Unraveling the Contributions to the Neuromelanin-MRI Contrast," *Brain Structure and Function* 225, no. 9 (2020): 2757–2774, https://doi.org/10.1007/s00429-020-02153-z.

18. M. Jokar, Z. Jin, P. Huang, et al., "Diagnosing Parkinson's Disease by Combining Neuromelanin and Iron Imaging Features Using an Automated Midbrain Template Approach," *NeuroImage* 266 (2023): 119814, https://doi.org/10.1016/j.neuroimage.2022.119814.

19. P. Liu, X. Wang, Y. Zhang, et al., "PENCIL Imaging: A Novel Approach for Neuromelanin Sensitive MRI in Parkinson's Disease," *NeuroImage* 291 (2024): 120588, https://doi.org/10.1016/j.neuroimage.2024.120588.

20. Q. Liu, P. Wang, C. Liu, et al., "An Investigation of Neuromelanin Distribution in *Substantia Nigra* and *Locus Coeruleus* in Patients With Parkinson's Disease Using Neuromelanin-Sensitive MRI," *BMC Neurology* 23, no. 1 (2023): 301, https://doi.org/10.1186/s12883-023-03350-z.

21. S. Wang, T. Wu, Y. Cai, Y. Yu, X. Chen, and L. Wang, "Neuromelanin Magnetic Resonance Imaging of Substantia Nigra and Locus Coeruleus in Parkinson's Disease With Freezing of Gait," *Frontiers in Aging Neuroscience* 15 (2023): 1060935, https://doi.org/10.3389/fnagi.2023.1060935.

22. Y. Wang, Y. Chen, D. Wu, et al., "Strategically Acquired Gradient Echo (STAGE) Imaging, Part II: Correcting for RF Inhomogeneities in Estimating T1 and Proton Density," *Magnetic Resonance Imaging* 46 (2018): 140–150, https://doi.org/10.1016/j.mri.2017.10.006.

23. K. H. Zou, S. K. Warfield, A. Bharatha, et al., "Statistical Validation of Image Segmentation Quality Based on a Spatial Overlap Index,"

Academic Radiology 11, no. 2 (2004): 178–189, https://doi.org/10.1016/S1076-6332(03)00671-8.

24. P. Trujillo, A. K. Smith, P. E. Summers, et al., "High-Resolution Quantitative Imaging of the Substantia Nigra," 2015 37th Annual International Conference of the IEEE Engineering in Medicine and Biology Society (EMBC), (2015): 5428–5431, https://doi.org/10.1109/EMBC.2015.7319619.

25. G. J. Stanisz, E. E. Odrobina, J. Pun, et al., "T1, T2 Relaxation and Magnetization Transfer in Tissue at 3T," *Magnetic Resonance in Medicine* 54, no. 3 (2005): 507–512, https://doi.org/10.1002/mrm.20605.

26. N. Hua, M. Horn, A. Aakil, S. Anderson, and H. Jara. "Incidental Magnetization Transfer in qMRI: Effects of Multi-Slice Imaging With Mixed-TSE," (2018): 2294.

27. T. Hilbert, D. Xia, K. T. Block, et al., "Magnetization Transfer in Magnetic Resonance Fingerprinting," *Magnetic Resonance in Medicine* 84, no. 1 (2020): 128–141, https://doi.org/10.1002/mrm.28096.

28. Y. Xing, A. Sapuan, R. A. Dineen, and D. P. Auer, "Life Span Pigmentation Changes of the Substantia Nigra Detected by Neuromelanin-Sensitive MRI," *Movement Disorders* 33, no. 11 (2018): 1792–1799, https://doi.org/10.1002/mds.27502.

Supporting Information

Additional supporting information can be found online in the Supporting Information section. **Figure S1:** Images illustrating the T1 correction procedure applied on a representative subject. A. Apparent T1 map (ms). B. B1 transmit field scale factor. C. T1 corrected map (ms). D. PD effective map (corrected for the inhomogeneities of the B1t field). **Figure S2:** Illustration of the ROIs drawn on the white matter (pink) and the grey matter (yellow). Five consecutive slices were selected for the ROI delineation. The slice shown on the left side is the lowest while the one on the right is the highest from the MT ON acquisition of a volunteer. **Table S1:** Paired sample *t*-test *p*-values and confidence intervals of the contrast ratio differences between frequencies (500, 1500, 2000, 4000, 10K, and 100K Hz). **Table S2:** Pairwise *t*-tests with Bonferroni correction for the contrast ratio differences between flip angles (5, 10, 20, 30, and 40 deg) for the case of magnetization transfer off. **Table S3:** Pairwise *t*-tests with Bonferroni correction for the contrast ratio differences between flip angles (5, 10, 20, 30, and 40 deg) for the case of magnetization transfer on. **Table S4:** Signed-ranks test with Bonferroni correction for the contrast to noise ratio differences between frequencies (500, 1500, 2000, 4000, 10K, and 100K Hz). **Table S5:** Signed-ranks test with Bonferroni correction for the contrast to noise ratio differences between flip angles (5, 10, 20, 30, and 40 deg) for the case of magnetization transfer off. **Table S6:** Signed-ranks test with Bonferroni correction for the contrast to noise ratio differences between flip angles (5, 10, 20, 30, and 40 deg) for the case of magnetization transfer on. **Table S7:** Pairwise *t*-tests with Bonferroni correction for the volume measurement differences between flip angles (5, 10, 20, 30, and 40 deg) for the case of magnetization transfer off. **Table S8:** Pairwise *t*-tests with Bonferroni correction for the volume measurement differences between flip angles (5, 10, 20, 30, and 40 deg) for the case of magnetization transfer on. **Figure S3:** Bland–Altman plot of volume measurements by the two ratters (R1 and R2) for each flip angle (5, 10, 20, 30, and 40 deg) considering both cases (magnetization transfer on and off).